ELSEVIER

Journal of Power Sources 104 (2002) 90–96

JOURNAL OF POWER SOURCES

www.elsevier.com/locate/jpowsour

Lithium alloy formation at bismuth thin layer electrode and its kinetics in propylene carbonate electrolyte

Wang Xianming*,[1], Tatsuo Nishina, Isamu Uchida

Department of Applied Chemistry, Graduate School of Engineering, Tohoku University, Aramaki-Aoba, Aoba-ku, Sendai 980-77, Japan

Received 26 March 2001; received in revised form 18 July 2001; accepted 6 August 2001

Abstract

The study on the formation of lithium alloying with Bi thin layer electrode and its kinetics was carried out in 1 mol/dm^3 $LiClO_4$/PC electrolyte. In situ XRD and chronopotentiometry results confirmed the formation of LiBi and Li_3Bi alloy phases with the open circuit potentials of 0.830 and 0.805 V, respectively. The formation of Li_3Bi alloy rather than LiBi alloy was found to be responsible for the mechanical degradation of Li–Bi alloy electrode. Lithium diffusion coefficient in LiBi alloy was evaluated to be in the order of 10^{-13} cm^2/s by ac impedance measurement. This smaller lithium diffusion coefficient in thin layer electrode than that in the common sheet electrode was attributed to the intrinsic properties of the thin layer electrode. Furthermore, a mechanism involving the adsorption process at the electrode surface was proposed for lithium alloying with bismuth.

Keywords: Lithium alloy; Bismuth thin layer electrode; In situ XRD; Kinetics; Lithium rechargeable batteries

1. Introduction

Due to the significant progress in integrated circuit microfabrication technology, some applications of lithium rechargeable batteries, such as cellular phone, camcorders, and laptop computers, are being operated at lower voltage range from 3 to 2.5 V. This makes it necessary to use power supplies with the same voltage range in order to save the voltage adjuster. For this reason, the study on lithium rechargeable batteries with lithium alloy as anode still looks reward because of the high theoretical energy density and positive potential plateau of lithium alloy anode [1–3].

So far, some data have been available for the thermodynamic and kinetic properties of the binary lithium alloy systems such as Li–Al, Li–Si, Li–Pb, Li–Sn, Li–Cd and Li–Zn, by determination of the open circuit potential and lithium diffusion coefficient [4–8]. Several groups also gave convincing reasons to show interesting prospects in the utilization of lithium alloy anodes [9–16]. Promising results in the improvement of cycling behavior of rechargeable lithium batteries were obtained with these materials as anodes. On the other hand, appreciable benefit is still not derived in commercialization up to now. To a certain extent, this may be attributed to the crumbling of the alloy electrodes which results from a significant volume or shape change involved in the lithium alloying processes [17–19].

To suppress the volume changes of lithium alloys during cycling, it has been considered to be effective to keep the thickness of the reaction layer in the order of a few micrometers [3,20–22]. Therefore, the thin layer electrode (approximately μm in thickness) becomes necessary in the studies of lithium alloying. Furthermore, an establishment of the electrochemical data for the thin layer electrode is also especially significant to develop the thin layer microbatteries with high energy density [20,23–25].

In this work, we studied on the lithium alloy formation at Bi thin layer electrode in 1 mol/dm^3 $LiClO_4$/PC electrolyte by both the electrochemical measurements (cyclic voltammetry, chronopotentiometry) and the surface analysis technique (in situ XRD). Furthermore, the kinetic data for this binary alloy were established by ac impedance measurement. The reason to choose bismuth is that it can form lithium alloy with a relative positive potential of about 0.8 V, which makes lithium ion batteries using bismuth as anode and $LiCoO_2$ as cathode have a lower voltage of about 3 V.

* Corresponding author. Tel.: +81-298-52-2299.
E-mail address: xianming_wang@hotmail.com (W. Xianming).
[1] Present address: On-board Power Engineering Group, Office of Research and Development, NASDA Tsukuba Space Center, 2-1-1 Sengen, Tsukuba, Ibaraki 305-8505, Japan.

0378-7753/02/$ – see front matter
PII: S0378-7753(01)00876-X

2. Experimental

2.1. Electrochemical measurement

In order to reduce the water level to a condition as anhydrous as possible, the vacuum line was used [26]. A five-hole container for setting the electrochemical cell was associated with the vacuum line. The cell atmosphere could be controlled in demand by the gas sources of argon which feed through gas purifiers. Usually argon atmosphere was maintained to prevent the cell from humidity. The electrode exchange could also be easily performed in course of experiment.

A 1 mol/dm^3 $LiClO_4$/PC electrolyte was used as received from Mitsubishi Chemical Corporation with a water content of <20 ppm. The electrolyte and Li reference electrode were sealed into glass ampoules to store. Before performing an experiment, they were led into electrochemical cell. The electrochemical measurement was carried out in a three-electrode configuration. A Pt sheet served as the counter electrode. All potentials were referred to Li^+ (1 mol/dm^3)/Li electrode.

Because it has been found in our previous work that no lithium alloying occurred for Ni [27], the Bi thin layer electrode was prepared by electroplating Bi onto Ni substrate in the plating bath as shown in Table 1 [28]. The thickness of thin layer electrode was evaluated by anodic stripping method in the same bath.

The electrochemical measurements were performed by an electrochemical interface (Solartron, 1287) coupled with a frequency response analyzer (Solartron, 1250). The water content in the electrolyte was monitored to be <20 ppm by Karl–Fischer titration (Mitsubishi, model CA-06) in course of measurements.

Table 1
Electroplating bath to prepare the Bi thin layer electrode

Metal	Composite	Current density (mA/cm^2)	Temperature (°C)
Bi	HCl (31 vol.%) $BiCl_3$ (7.93 g/dm^3)	5	50–60

2.2. In situ XRD measurement

A commercial diffractometer (XD-D1, Simadzu) was used. The collimated X-ray beam (Cu Kα) was toward the working electrode surface at a fixed, glancing angle (8° from the surface). The cell was assembled in the argon glove box, as shown in Fig. 1. A Teflon type film (FEP100A, 25 μm in thickness), which led to the distinct peaks at 2θ angles of 31.37 and 36.33° in XRD pattern, was used as the window attached to the cell by an O-ring. Two lithium foils served as the counter and reference electrodes, respectively.

The disk covered with Bi thin layer was connected to a movable stainless rod for electric contact. In usual electrochemical measurement, the disk was placed at a normal position closed to reference electrode, while in XRD measurements, the disk was pressed onto the window film to remove the electrolyte between the disk surface and the window film. To ensure this operation, the inner cell pressure was adjusted by the use of syringe.

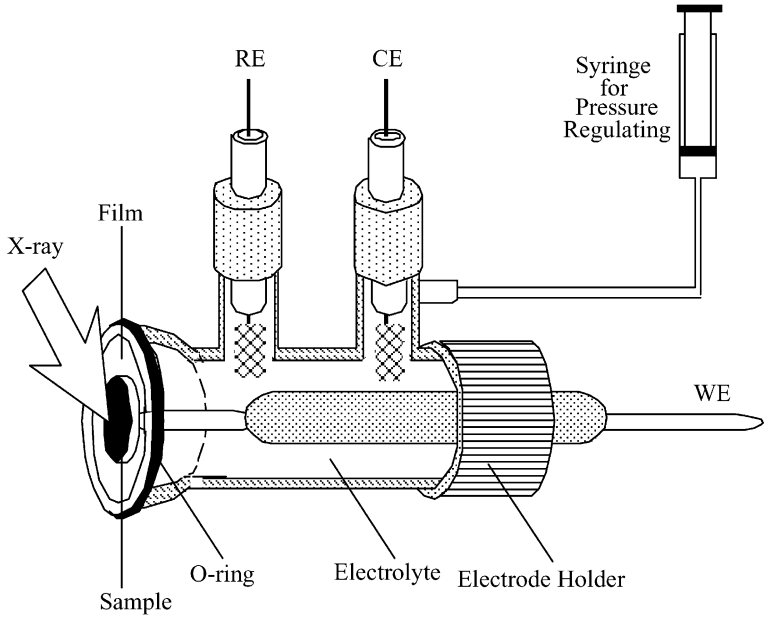

Fig. 1. The electrochemical cell for in situ XRD measurement.

3. Results and discussion

3.1. Formation of lithium alloys

According to the phase diagram of Li–Bi alloy system, LiBi and Li_3Bi alloy phases may be formed at ambient temperature [29]. To identify the electrochemical formation of Li–Bi alloy system, in situ XRD was performed after applying the constant potentials to Bi thin layer electrode.

Fig. 2 shows in situ XRD patterns for Bi thin layer electrode. First, the potentials negative of OCV were applied to the Bi thin layer electrode. The XRD patterns gave the peaks at 2θ angles of 27.34, 38.07 and 39.81°, respectively, corresponding to the (1 0 2), (0 1 4) and (1 1 0) planes of Bi at the potential positive of 0.8 V. At 0.8 V, the distinct peaks at 2θ angles of 21.19, 26.79, 34.42 and 38.66° occurred, respectively, corresponding to the (0 0 1), (1 1 0), (1 1 1) and (2 0 0) planes of LiBi alloys, and the peaks for Bi were declined. After held at 0.78 V, the electrode consisted of only LiBi alloy. The open circuit potential for the LiBi alloy was 0.830 V. The peaks of (1 1 1), (2 0 0) and (2 2 0) planes of Li_3Bi alloy at 2θ angles of 23.21, 26.70 and 38.07° were observed at 0.76 V, and the peaks for LiBi alloy disappeared at 0.72 V. The open circuit potential for Li_3Bi alloy was evaluated to be 0.805 V. There was no further change in XRD pattern at the potential negative of 0.72 V. Then the oxidation of Li_3Bi alloy was performed by applying the potentials positive of 0.72 V. The peaks for LiBi alloy and Bi phases were simultaneously observed at 0.84 V, suggesting that the oxidations of LiBi and Li_3Bi alloy phases occurred at so near potentials as to be difficult to characterize each other. After the potential was held at 0.84 V for a long time, the LiBi and Li_3Bi alloy phases disappeared, and the electrode consisted of only Bi. These results implied that lithium may be reversibly alloyed with Bi to form LiBi and Li_3Bi alloys via the reactions

$$Li^+ + Bi + e \rightarrow LiBi \quad (1)$$

$$2Li^+ + LiBi + e \rightarrow Li_3Bi \quad (2)$$

The formation of lithium alloys was also identified by chronopotentiometry. Fig. 3 shows the potential decay curve of Bi thin layer electrode in 1 mol/dm^3 $LiClO_4$/PC electrolyte. A low current density of 0.5 μA/cm^2 was applied in order to obtain the equilibrium phase. For Bi electrode, two potential plateaus were observed at 0.815 and 0.781 V with the compositions spanning from 0 to 1.2 and 1.2 to 3.0 lithium per mole, respectively, corresponding to the two-phase coexistence states of Li and LiBi, LiBi and Li_3Bi. Because the plateaus for these two alloys maintained over the appreciable ranges of lithium composition, the battery systems using these alloys as anode materials may operate at the constant cell voltage during the charge and discharge cycles.

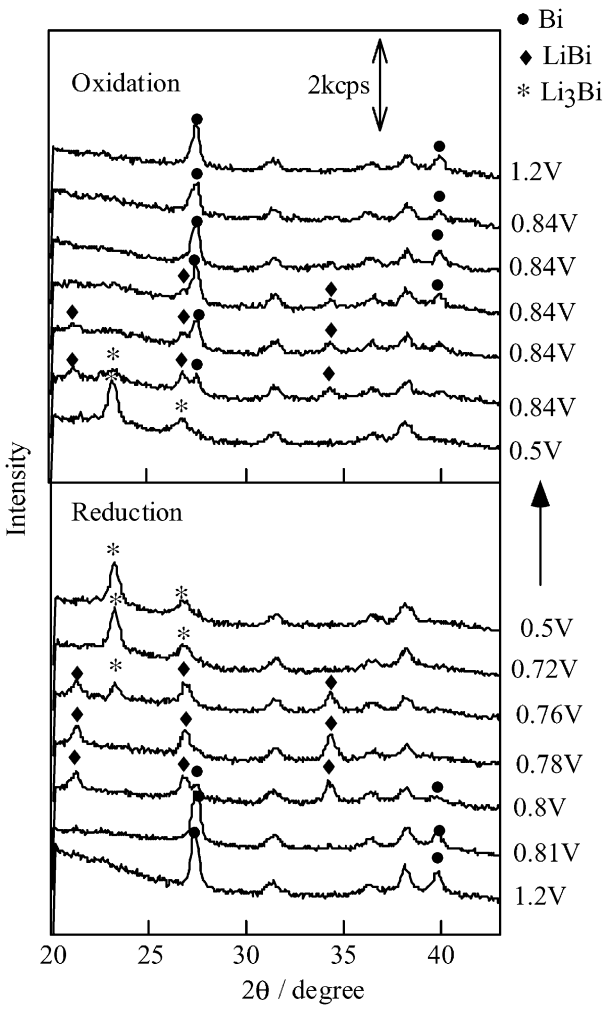

Fig. 2. In situ XRD patterns of Bi thin layer electrode (1 μm in thickness) after being hold at various potentials in 1 mol/dm^3 $LiClO_4$/PC electrolyte.

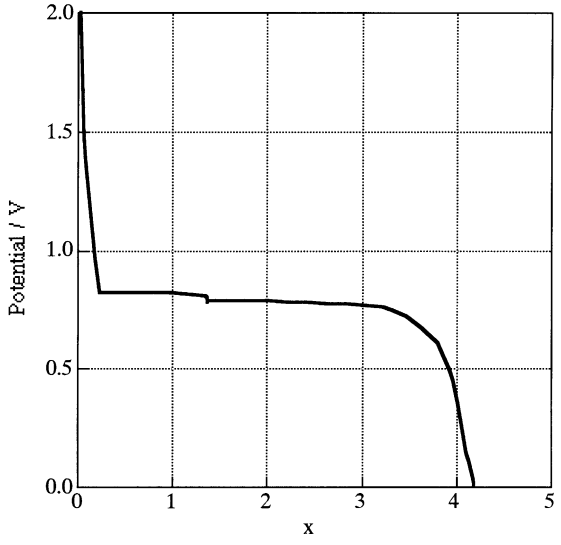

Fig. 3. The charge curves at Bi thin layer electrode (thickness: 0.2 μm, area: 0.39 cm^2) in 1 mol/dm^3 $LiClO_4$/PC electrolyte. Current density: 0.5 μA/cm^2.

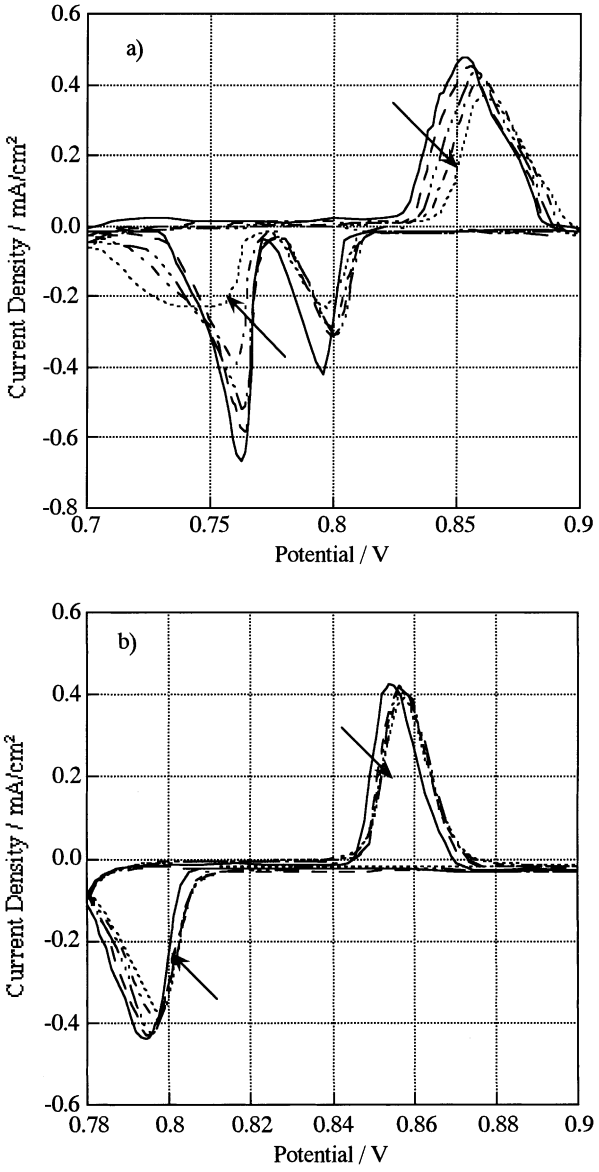

Fig. 4. Cyclic voltammograms with the reversed potentials of (a) 0.70 V and (b) 0.78 V at Bi thin layer electrode (thickness: 0.2 μm, area: 0.39 cm^2) in 1 mol/dm^3 $LiClO_4$/PC electrolyte. Scan rate: 0.1 mV/s.

Another attempt was made to evaluate the effect of cycle number on Li–Bi alloy formation. In Fig. 4a, the potential was initially set to 1 V, which yielded no appreciable current. Then the potential was scanned to 0.70 V and cycled linearly with time between 0.70 and 1 V at 0.1 mV/s. For the first cycle, two cathodic peaks were observed at 0.78 and 0.73 V, corresponding to the formation of LiBi and Li_3Bi alloys, respectively. Apparently, only one wide anodic wave was observed at the potential of 0.83–0.90 V. This observation confirmed the above explanation that the oxidation of LiBi and Li_3Bi alloys occurred at the very near potential range as verified by in situ XRD result. Three significant changes may be identified with increasing cycle number. First, the peak current density declined rapidly. Second, the peak potential moved greatly for both the oxidation and reduction processes. Third, the peaks for the Li_3Bi formation broadened gradually. It has been reported that the cycling behavior of Li_3Bi alloy was related to the mechanical degradation of the electrode resulting from the significant volume expand (177%) with lithium incorporation into bismuth [17]. Therefore, the above observed phenomena seem reasonable to be attributed to the crystalline structure destroy with cycle number.

On the other hand, Fig. 4b shows the cyclic voltammograms cycled linearly between 0.78 and 1 V at 0.1 V/s, corresponding to the formation of only LiBi alloy phase. It was noted that only slight changes in the peak current density and the peak potential occurred with the lithium insertion process for LiBi alloy as compared with that for Li_3Bi alloy. This implied that the formation of Li_3Bi alloy rather than LiBi alloy was responsible for the mechanical degradation of the Li–Bi alloy electrode. Furthermore, the volume discharge capacity and coulomb efficiency of LiBi alloy electrode were calculated to be 731 mAh/cm^3 and 91%, respectively, at first cycle. These characteristics make LiBi phase a merit of the potential application as anode material for lithium rechargeable batteries.

3.2. Kinetics of lithium alloying

Fig. 5 shows the formation of LiBi alloy at Bi thin layer electrode by potential sweep method. The potential was initially set to 1 V, then cathodically scanned to 0.79 V and opened to a release state. A cathodic wave was observed, implying the formation of LiBi alloy phase. In order to realize the lithium concentration leveling in alloy phase, the release state was held to an enough long duration. Finally,

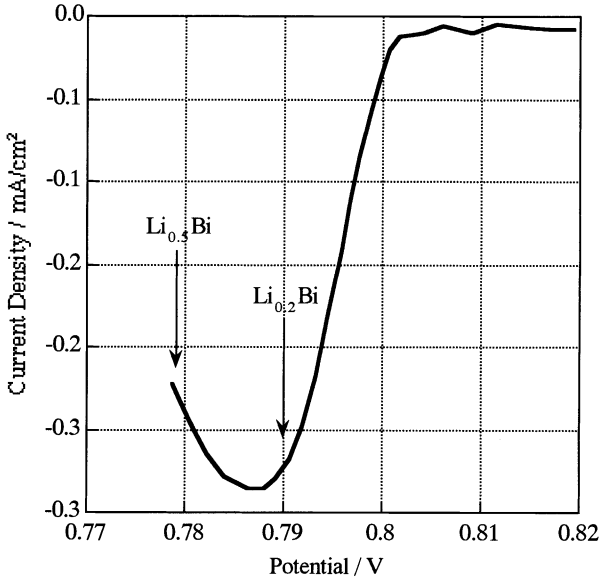

Fig. 5. Formation of LiBi alloys with different compositions at Bi thin layer electrode (thickness: 0.2 μm, area: 0.39 cm^2) in 1 mol/dm^3 $LiClO_4$/PC electrolyte. Scan rate: 0.1 mV/s.

the potential of LiBi alloy electrode kept constant at 0.83 V, suggesting the two-phase coexistence of Bi and LiBi alloy.

The total charge Q for lithium alloying was evaluated to be 9.05×10^{-3} C by the integration of the cathodic wave. Therefore, the bulk lithium concentration C^* was estimated to be 1.20×10^{-2} mol/cm^3 by the following equation:

$$C^* = \frac{Q}{nFAl} \tag{3}$$

where F denotes Faraday constant, A the area of Bi electrode (0.39 cm^2), and l is the thickness of Bi electrode (0.2 μm). Furthermore, the average composition of this lithium alloy was evaluated to be $Li_{0.25}Bi$ from the quantity of plated Bi (3.7×10^{-7} mol).

The Cole–Cole plot of this formed lithium alloy electrode is shown in Fig. 6, which may be divided into two parts of semi-circular and linear port, respectively, corresponding to the frequency ranges of 1.3 kHz–0.5 Hz and 0.07–0.01 Hz. The amplitude of the sinusoidal perturbation was set to 5 mV from the open circuit voltage (0.83 V) of the alloy electrode in order to suppress the variation in the electrode composition during the impedance measurement. The straight line varied well with a slope of 45°, indicative of a diffusion process.

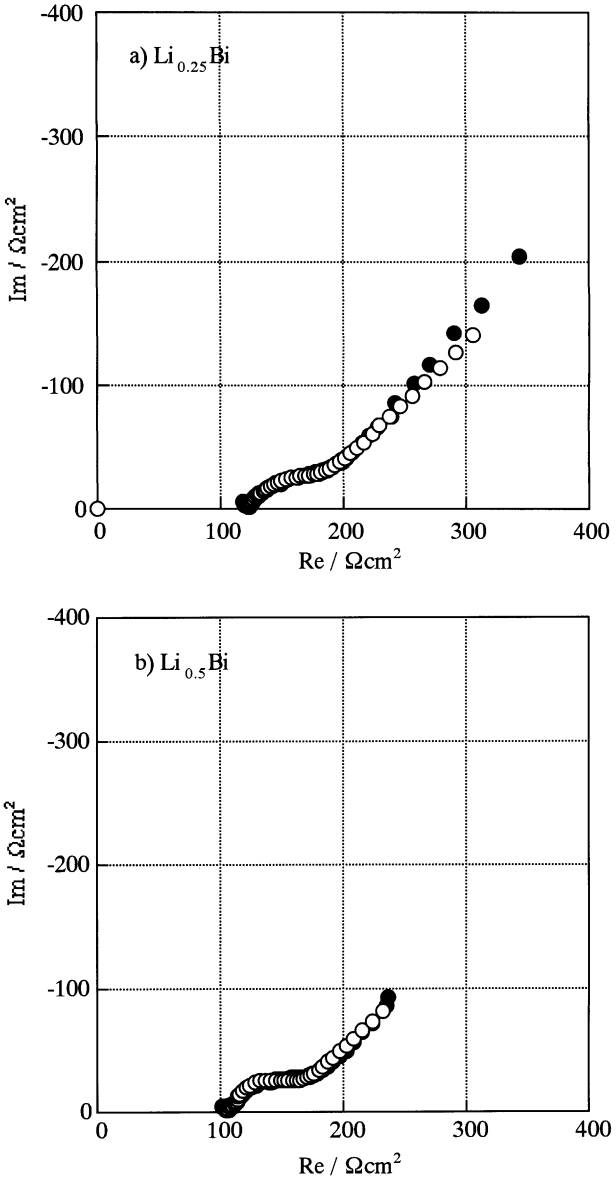

Fig. 6. Cole–Cole plots (a) and the fitting results (b) of LiBi alloys formed in Fig. 5. Frequency: 10 kHz–0.01 Hz, amplitude: 5 mV.

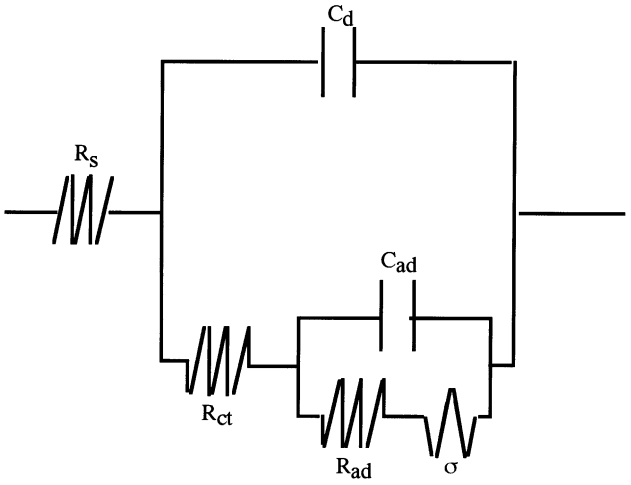

Fig. 7. Equivalent circuit for electrochemical reaction involving adsorption and desorption used to fit the impedance results of Fig. 6.

In order to extract the kinetic information, various designated equivalent circuits were used to fit the measured impedance spectra. The good agreement was obtained between the experimental data and simulated curves of the equivalent circuit involving adsorption and desorption, as illustrated in Fig. 7 [30,31]. Here R_s is assigned to the ohmic resistance of the electrolyte, C_d the differential capacitance of the double layer, R_{ct} the charge transfer resistance for lithium redox reaction, σ an impedance resulting from the diffusion of lithium in the lithium alloy electrode, R_{ad} adsorption resistance, C_{ad} pseudo-capacitance of adsorption layer, respectively. The main kinetic parameters were obtained from the fitting result and summarized in Table 2. Lithium diffusion coefficient D in $Li_{0.25}Bi$ alloy was evaluated to be 2.0×10^{-13} cm^2/s.

By the same method, the kinetic parameters of LiBi alloy with the average composition of $Li_{0.5}Bi$ was also evaluated and summarized in Table 2. Though the average composition of $Li_{0.5}Bi$ alloy was different from that of $Li_{0.25}Bi$ alloy, these two LiBi alloys had almost the same lithium diffusion coefficient and exchange current density i_0.

Table 2
Kinetic parameters for LiBi alloy formation obtained from ac impedance as shown in Fig. 6

	$D \times 10^{13}$ (cm^2/s)	R_{ct} (Ω cm^2)	$C_d \times 10^4$ (F)	$C_{ad} \times 10^3$ (F)	R_{ad} (Ω cm^2)	i_0 (mA/cm^2)
$Li_{0.25}Bi$	2.0	22.4	4.12	1.36	26.5	0.53
$Li_{0.5}Bi$	1.4	11.2	4.96	1.94	38.4	0.52

3.3. Discussion

It was noted that lithium diffusion coefficient in LiBi thin layer electrode was two order smaller than that in a common lithium alloy sheet electrode, which is about 10^{-8} cm^2/s [13]. In fact, this finding were also reported by the other authors who used thin layer or film electrodes [20,32–35]. Though the convincible evidence has not been still given to understand the small lithium diffusion coefficients in thin layer electrodes, it may be generally influenced by the intrinsic properties of the thin layer. Nicholson attributed the small lithium diffusion coefficient in thin layer electrode to the less grain boundaries in the thin layer electrodes than in the common sheet electrodes, because lithium diffused more faster through the grain boundaries than the inner grain [35]. Julien correlated the small lithium diffusion coefficient in thin layer electrode to the orientation, crystallographic imperfection and porosity of the thin layer [20]. For a sheet electrode with low lithium diffusion coefficient, lithium may deposited on the electrode surface to promote the lithium dendrite formation. However, the diffusion distance in the thin layer electrode used in this work is very small, and the application of the thin layer lithium alloy electrode in microbatteries generally requires low current drain of about nA/cm^2. Therefore, it may be believed that small lithium diffusion coefficient will not address significant problem.

Due to the good agreement between the impedance results of these lithium alloys and simulated curves fitted from the equivalent circuit involving adsorption and desorption, it seems reasonable to suppose that the formation of Li–Bi alloys follows the mechanism involving the adsorption process at the electrode surface.

1. Diffusion of lithium ion from bulk electrolyte to Bi electrode

$$Li^+_{bulk} \rightarrow Li^+_{electrode} \quad (4)$$

2. Adsorption of lithium ion onto the surface of Bi electrode, which reduces the energy barrier of lithium reduction reaction, like the situation of under potential deposition

$$Li^+_{electrode} \rightarrow Li^+_{ad}(Bi) \quad (5)$$

3. Reduction of adsorbed lithium ion

$$Li^+_{ad}(Bi) + e \rightarrow Li_{ad}(Bi) \quad (6)$$

4. Lithium diffusion to the inner electrode

$$Li_{ad}(Bi) \rightarrow Li{-}Bi \quad (7)$$

In fact, Li and Pons have corroborated that the lithium adsorption/desorption occurred in course of lithium alloying with Au using far-infrared spectroscopy [36]. To a certain extent, this supports the above explanation for the formation of Li alloys.

Since lithium alloy electrode experiences the volume change with cycle, it is easily considered that the film of thin layer lithium alloy electrode may be peeled off the substrate and hence cause capacity fade. However, the CV result in Fig. 4b showed good cycling performance for LiBi alloy electrode, suggesting that the film was still attached on the substrate. To a certain extent, this gave the evidence that the thin layer electrode is effective to suppress the volume change of lithium alloy electrode with cycle.

4. Conclusions

The study on the formation of lithium alloying with Bi thin layer electrode and its kinetics was carried out in 1 mol/dm^3 $LiClO_4$/PC electrolyte. From the foregoing results and discussion, the following conclusions can be drawn.

1. The formation of Li–Bi alloys at the applied potential was verified by in situ XRD and chronopotentiometry. LiBi and Li_3Bi alloy phases were confirmed with the open circuit potentials of 0.830 and 0.805 V, respectively. The cyclic voltammometry results disclosed that the formation of Li_3Bi alloy rather than LiBi alloy was responsible for the mechanical degradation of Li–Bi alloy electrode.
2. Lithium diffusion coefficient in LiBi alloy was evaluated to be in the order of 10^{-13} cm^2/s by ac impedance measurement. The smaller lithium diffusion coefficient in thin layer electrode than that in the common sheet electrode may be attributed to the intrinsic properties, such as the orientation, crystallographic imperfection, less grain boundary and porosity of the thin layer electrode.
3. The formation of Li–Bi alloy may be supposed to follow the mechanism involving the adsorption process at the electrode surface.

References

[1] Y. Idota, T. Kubota, A. Matsufuji, Y. Maekawa, T. Miyasaka, Science 276 (1997) 1395.
[2] R.A. Huggins, J. Power Sources 81/82 (1999) 13.
[3] J.O. Besenhard, J. Yang, M. Winter, J. Power sources 68 (1997) 87.
[4] J. Wang, P. King, R.A. Huggins, Solid States Ionics 20 (1986) 185.
[5] J. Wang, I.D. Raistrick, R.A. Huggins, J. Electrochem. Soc. 133 (1986) 457.
[6] A. Anani, S. Crouch-Baker, R.A. Huggins, J. Electrochem. Soc. 134 (1987) 3098.
[7] A. Anani, S. Crouch-Baker, R.A. Huggins, in: A.N. Dey (Ed.), Proceedings of the ECS Symposium on Lithium Batteries, Pennington, NJ, 1987, p. 365.
[8] C.J. Wen, Ph.D. Dissertation, Stanford University, 1980.
[9] I.A. Courtney, J.R. Dahn, J. Electrochem. Soc. 144 (1997) 2943.
[10] A.S. Baranski, W.R. Fawcett, J. Electrochem. Soc. 129 (1982) 901.
[11] I. Epelboin, M. Froment, M. Garreau, J. Thevenin, D. Warin, J. Electrochem. Soc. 127 (1980) 2100.
[12] S. Biallozor, M. Lieder, J. Electrochem. Soc. 140 (1993) 2537.
[13] S. Machill, D. Rahner, J. Power Sources 54 (1995) 428.
[14] H. Tsukamoto, Japan Patent, 03280363 (1991).
[15] H. Yoshida, Japan Patent, 04220961 (1992).
[16] Y. Takada, K. Sasaki, Japan Patent, 07022017 (1995).

[17] D. Fauteux, R. Koksbang, J. Appl. Electrochem. 23 (1993) 1.
[18] J. Wolfenstine, D. Foster, J. Read, W.K. Behl, W. Luevke, Proc. Electrochem. Soc. 99 (25) (2000) 172.
[19] M. Winter, J.O. Bensenhard, J.H. Albering, J. Yang, M. Wachtler, Prog. Batteries Battery Mater. 17 (1998) 208.
[20] C. Julien, in: G. Pistoia (Ed.), Lithium Batteries/New Materials, Developments and Perspectives, Elsevier, Amsterdam, 1994, p. 167.
[21] J. Yang, Y. Takeda, N. Imanishi, T. Ichikawa, O. Yamamoto, J. Power Sources 79 (2) (2000) 220.
[22] J. Yang, J.O. Bensenhard, M. Winter, Proc. Electrochem. Soc. 97 (18) (1997) 350.
[23] R.P. Raffaelle, J.D. Harris, D. Hehemann, D. Scheiman, G. Rybicki, A.F. Hepp, J. Power Sources 89 (2000) 52.
[24] R.J. Jasinski, High Energy Batteries, Plenum Press, New York, 1967.
[25] D.O. Hobson, US Patent, 5705293 A (1998).
[26] X. Wang, T. Nishina, I. Uchida, Surf. Technol. 46 (1995) 941 (in Japanese).
[27] X. Wang, T. Nishina, I. Uchida, Electrochemistry 2 (1999) 145 (in Japanese).
[28] S. Asahara, Handbook of Metal Surface Technolog, Nikkan Kogyo Shinbun, 1981 (in Japanese).
[29] S. Nagasaki, Databook of Metal, Maruzen, 1983 (in Japanese).
[30] R. Sylvie, P. Cowache, P. Boncorps, J. Vedel, Electrochim. Acta 38 (1993) 2043.
[31] E.D. Chabala, B.H. Harji, T. Rayment, M.D. Archer, Langmuir 8 (1992) 2028.
[32] A.A. van Zomeren, J.H. Koegler, J. Schoonman, P.J. van der Put, Solid State Ionics 53–56 (1992) 333.
[33] K. Kanehori, Y. Ito, F. Kirino, K. Miyauchi, T. Kudo, Solid State Ionics 9/10 (1983) 1445.
[34] N. Kumagai, Y. Koishikawa, S. Komaba, N. Koshiba, J. Electrochem. Soc. 146 (1999) 3203.
[35] M.M. Nicholson, J. Electrochem. Soc. 121 (1974) 734.
[36] J. Li, S. Pons, Langmuir 2 (1986) 297.